Advanced Composite Materials
Publication details, including instructions for authors and subscription information:
http://www.tandfonline.com/loi/tacm20

# Analytical modeling and in situ measurement of void formation in liquid composite molding processes

Sébastien Gueroult[a], Aurélie Lebel-Lavacry[a], Chung Hae Park[a], Laurent Bizet[a], Abdelghani Saouab[a] & Joël Bréard[a]
[a] Laboratoire d'Ondes et Milieux Complexes, UMR 6294 CNRS, University of Le Havre, 53 rue de Prony, 76058 Le Havre, France
Published online: 29 Nov 2013.

To cite this article: Sébastien Gueroult, Aurélie Lebel-Lavacry, Chung Hae Park, Laurent Bizet, Abdelghani Saouab & Joël Bréard (2014) Analytical modeling and in situ measurement of void formation in liquid composite molding processes, Advanced Composite Materials, 23:1, 31-42, DOI: 10.1080/09243046.2013.862383

To link to this article: http://dx.doi.org/10.1080/09243046.2013.862383

*Advanced Composite Materials*, 2014
Vol. 23, No. 1, 31–42, http://dx.doi.org/10.1080/09243046.2013.862383

Taylor & Francis
Taylor & Francis Group

# Analytical modeling and *in situ* measurement of void formation in liquid composite molding processes

Sébastien Gueroult, Aurélie Lebel-Lavacry, Chung Hae Park*, Laurent Bizet, Abdelghani Saouab and Joël Bréard

*Laboratoire d'Ondes et Milieux Complexes, UMR 6294 CNRS, University of Le Havre, 53 rue de Prony, 76058 Le Havre, France*

(*Received 17 January 2013; accepted 4 April 2013*)

Liquid composite molding processes are widely accepted in the aeronautic industry to manufacture large and complex structural parts. In spite of their cost-effectiveness, void defects created during the manufacturing process are a major issue of these processing techniques because they have detrimental effects on the mechanical performance. The reliable modeling is still a difficult task and experimental observations are usually adopted for the analysis of void formation mechanism, however, because many different physics are simultaneously involved during the mold filling process and the resin curing process. The complexity of the void formation physics implies the need for an *in situ* measurement of void formation not in the final part but in the mold filling procedure during the manufacturing process to better understand the void mechanism. In this regard, we present a sensor system measuring the electric conductivity for the *in situ* monitoring of void formation during the mold filling process. We also propose a theoretical model to predict void formation in a quantitative way with the properties of the resin and the fiber reinforcement. The model prediction is compared with the experimental data obtained by the sensor system to validate the model.

**Keywords:** liquid composite molding processes; void defects; *in situ* measurement; theoretical model; electric conductivity



## 1. Introduction

Liquid composite molding processes such as the resin transfer molding and the vacuum-assisted resin transfer molding process are attracting great attention from the aeronautic industry as cost-effective alternatives to the conventional prepreg techniques. In these processes, dry fiber reinforcement preplaced in the mold, called preform, is impregnated by a liquid resin which is subsequently cured to obtain a final product. Void type defects generated during the manufacturing process, however, are a critical issue in the use of these techniques because they degenerate the mechanical performance of a final product.[1–6] Air entrapment by non-uniform resin flow at the flow front is regarded as the main source of void generation in the resin transfer molding process whereas other phenomena such as volatile generation and premature resin gelation during the curing process also induce the void formation.[7–11]

*Corresponding author. Also at: Department of Polymers and Composites Technology & Mechanical Engineering, Ecole Nationale Supérieure des Mines de Douai, 941 rue Charles Bourseul, 59500 Douai, France. Email: chung-hae.park@mines-douai.fr

In general, the heterogeneous microstructure of fiber preform is considered to be the main reason for the non-uniform resin flow at the flow front.[11] Frequently, high count tow fabrics are used as fiber preform to enhance the mechanical properties. Hence, two different sizes of pore are observed in the fabric microstructure, viz. very tiny pores inside the tow and relatively large open gap between the tows (see Figure 1(a)). As the pore size is different, the flow characteristic as well as the flow resistance is different at each zone. The viscous flow is dominant at the open gap between the tows and the capillary wicking is the main flow nature at the micropores inside the tow. Therefore, air is entrapped either inside the tow or in the open gap between the tows depending on the relative ratio of the viscous flow to the capillary wicking. It has been reported that the void formation at the flow front for a specific preform, regardless of resin type, can be correlated with a dimensionless number called the modified capillary number which is a ratio of viscous force to surface tension.[11–14]

$$Ca^* = \frac{\mu \cdot u}{\gamma \cdot \cos\theta} \tag{1}$$

where $\mu$ is the resin viscosity, $u$ is the resin velocity, $\gamma$ is the surface tension, and $\theta$ is the contact angle.

It has been well known that the resin velocity is an important process parameter to influence the void formation. If the resin velocity is high and the corresponding

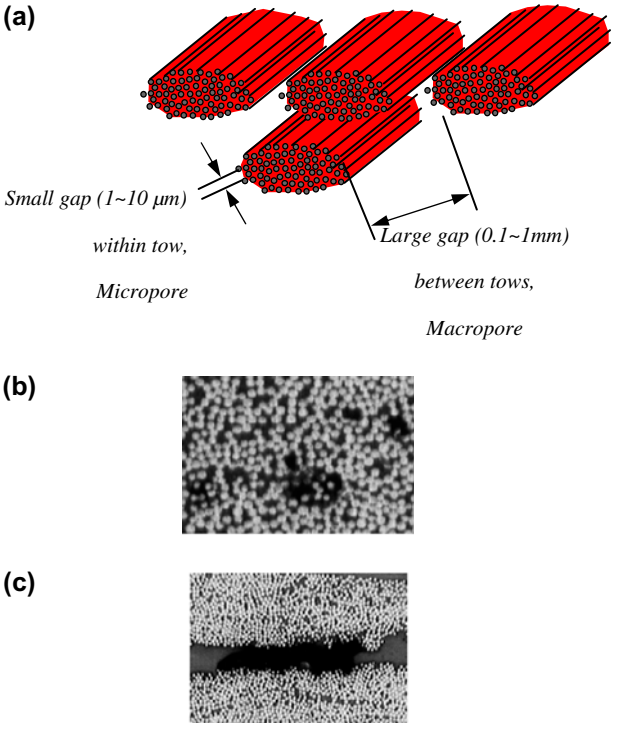


Figure 1. Textile reinforcement microstructure and void images in a final part. (a) Two different length scales in double-scale porous textile reinforcements. (b) Void inside the fiber tow. (c) Void between the fiber tows.

modified capillary number is high, air voids are generated inside the tow (see Figure 1(b)). If the resin velocity is low and the corresponding modified capillary number is low, air voids are generated at the open gap between the tows (see Figure 1(c)). In general, there exists an optimal capillary number to minimize the void formation. This implies that the void formation can be reduced by process optimization because modified capillary number is proportional to resin velocity which can be controlled by the process conditions.[15] Practical issues lie in, however, the difficulties in the prediction of the correlation between void content and modified capillary number and in the reliability of experimental measurement. Numerous experimental measurements are required to obtain the relation between modified capillary number and void content for a given preform. Hence, a theoretical model to predict the void content in terms of material properties and process condition may be useful for the process optimization. As an experimental technique, *in situ* visualization technique has been generally employed to establish such a relation.[11–14] As a matter of fact, *in situ* visual observation measurement is tedious and lacks in qualitative accuracy. To obtain the void content, more reliable are the microscopic image analysis and the apparent density measurement by matrix burning of cured samples.[16,17] They can lead to errors in interpreting the experimental results, however, because the void distribution in the mold filling process and that in the final cured part can be different. Actually, the void formation mechanism that can be interpreted by modified capillary number is the phenomenon that takes place at the resin flow front during the mold filling process and the air voids continue to change their sizes (i.e. bubble compression or expansion) and positions (i.e. void migration) with time.[18,19]

For the convenience, some researchers describe the void evolution mechanism during the manufacturing process by the parameter called degree of saturation which is a ratio of volume occupied by liquid to total pore volume. Introducing the concept of degree of saturation, the progressive impregnation of a preform by resin can be more effectively described. The degree of saturation is also introduced in the governing equation of resin flow in the porous preform to better model the interrelation among the void content, permeability and global resin pressure field.[20–22] Therefore, the degree of saturation at the moment of void creation during the mold filling process is indispensable information for a better interpretation of resin flow and void formation mechanism.

In the subsequent chapters, we present an analytical equation for void formation in terms of resin properties and preform properties, in the case of rectilinear resin injection. We also propose a sensor system to measure the degree of saturation during the mold filling process. Model predictions and experimental measurement results are compared to validate the proposed model.

## 2. Analytical model

In the previous work, we proposed a numerical model to predict the void formation at the flow front.[18] In this chapter, this model is briefly introduced and an analytical solution in the case of rectilinear injection into a unidirectional mat is derived.

The basic principle of the void formation modeling is to compare two time scales for the resin to transverse a single tow length in the channel between the tows and inside the tow at the flow front. In the macroscopic scale, the resin pressures field is obtained by the continuity equation and Darcy's law. Then, we compare two resin flows at the flow front in the microscopic scale: the flow in the macropore or the channel zone which is the open gap between the fiber tows and the flow in the micropore

which is the tiny space between the fiber filaments inside the tow. The resin flow in the macropore or the channel is modeled by Darcy's law using the global resin pressure gradient and the equivalent macropore permeability.

$$u_M = \frac{\mathrm{d}l_C}{\mathrm{d}t} = -\frac{K_M}{\mu}\frac{\partial P}{\partial x} \tag{2}$$

where $u_M$ is the resin velocity in the channel, $l_C$ is the resin flow front location from the tip of the tow in the channel, and $K_M$ is the equivalent macropore permeability (see Figure 2).

The resin flow in the micropore or inside the tow is computed by Darcy's law considering the fiber tow permeability and the capillary pressure at the resin-air interface.

$$u_m = \frac{\mathrm{d}l_T}{\mathrm{d}t} = -\frac{1}{1-V_{f,T}}\frac{K_T}{\mu}\left(\frac{\partial P}{\partial x} - \frac{P_{\mathrm{cap}}}{l_T}\right) \tag{3}$$

where $u_m$ is the resin velocity in the tow, $l_T$ is the resin penetration depth inside the tow from the tip of the tow, $V_{f,T}$ is the fiber volume fraction inside the tow, $K_T$ is the permeability of the tow, and $P_{\mathrm{cap}}$ is the capillary pressure at the resin-air interface inside the tow (see Figure 2).

A fiber tow can be regarded as a unidirectional mat. Hence, Gebart's model for permeability of unidirectional mats is used to obtain the tow permeability assuming the hexagonal fiber array.[23] Capillary pressure in the tow is obtained by a following relation.[24]

$$P_{\mathrm{cap}} = \left(\frac{F}{D_f}\right)\frac{V_{f,T}}{1-V_{f,T}}\gamma\cdot\cos\theta \tag{4}$$

where $D_f$ is the fiber diameter and $F$ is the shape factor (2 for the transverse direction and 4 for the longitudinal direction).

Then, times scales for the resin to travel through a single tow length are computed in the channel and in the tow, respectively. The void contents in the channel and in the tow can be obtained by following equations (see Figure 3).

$$\text{Figure 3(a), If } \Delta t_T > \Delta t_C\text{: } V_{a,T} = h_{v,T}\cdot v_T\cdot(1-V_{f,T})\left(1-\frac{\Delta t_C}{\Delta t_T}\right),\ V_{a,C} = 0 \tag{5}$$

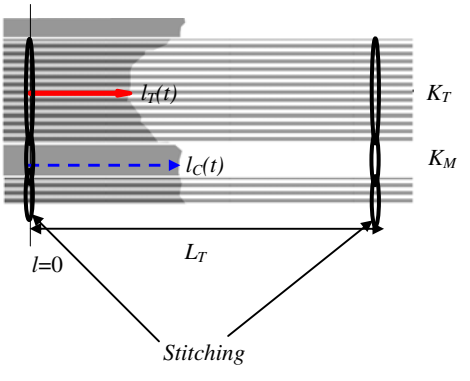


Figure 2. Schematic of two different flows in the channel and inside the tow at the flow front.

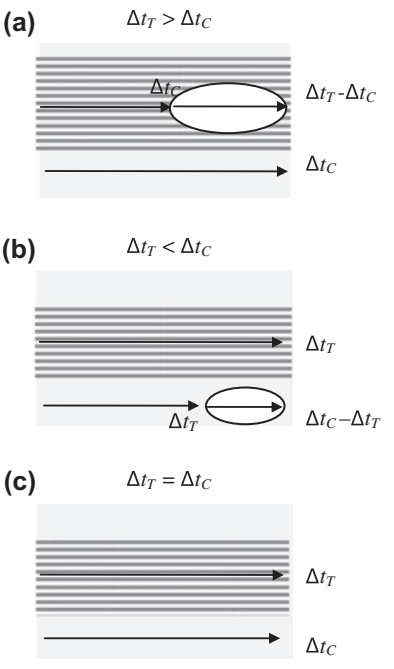


Figure 3. Void formation mechanism. (a) Void formation inside the tow. (b) Void formation in the channel between the tows. (c) No void formation.

$$\text{Figure 3(b), If } \Delta t_T < \Delta t_C\text{: } V_{a,C} = h_{v,C} \cdot (1 - v_T)\left(1 - \frac{\Delta t_T}{\Delta t_C}\right),\ V_{a,T} = 0 \tag{6}$$

$$\text{Figure 3(c), If } \Delta t_T = \Delta t_C\text{: } V_{a,C} = V_{a,T} = 0 \tag{7}$$

where $\Delta t_T$ is the time scale for the resin to travel a single tow length in the tow ($L_T$), $\Delta t_C$ is the time scale for the resin to travel a single tow length in the channel, $V_{a,T}$ is the void content in the tow, $V_{a,C}$ is the void content in the channel, $v_T$ is the tow volume fraction, $h_{v,T}$ is the void shape factor in the tow, and $h_{v,C}$ is the void shape factor in the channel.

As can be seen in the above relations, the void content can be expressed in terms of a ratio of two time scales. Assuming that the global resin pressure gradient is not changed during the resin impregnation in a single tow at the flow front, an analytic solution can be derived for the ratio of these two time scales.

$$\frac{\Delta t_T}{\Delta t_C} = \frac{K_M}{K_T} \cdot (1 - V_{f,T})\left[1 - \frac{F \cdot K_M \cdot V_{f,T}}{D_f \cdot (1 - V_{f,T}) \cdot L_T \cdot Ca^*} \ln\left(\frac{Ca^* \cdot D_f \cdot (1 - V_{f,T}) \cdot L_T}{F \cdot K_M \cdot V_{f,T}} + 1\right)\right] \tag{8}$$

As stated previously, it has been known that the void formation can be correlated with modified capillary number for a specific preform regardless of resin properties.[11–14] As shown in the above relation, all the resin properties are lumped into modified capillary number. Consequently, we can confirm that the void content can be decided exclusively by modified capillary number and the fabric microstructure parameters.

## 3. Experimental methods

### 3.1. Materials and mold setup

The mold used to conduct a resin injection consists of a lower steel plate and an upper glass plate for the visualization of the liquid flow. The dimensions of the rectangular mold cavity are 0.0028 m (thickness), 0.550 m (length), and 0.140 m (width). The lower steel plate is marked by several sensors to measure electrical voltage between a top electrode and a bottom electrode at different positions (0.04, 0.160, 0.280, and 0.390 m). The electrical voltage sensors are arrayed with different intervals to avoid a superposition with other sensors such as pressures sensors and heat flux sensors.

As a fiber preform, a stack of unidirectional stitched glass mats from Chomarat was employed. The areal weight is 646 g/m$^2$ and the stitching density is 4.9/cm$^2$. A single tow contains 2000 fiber filaments and the mean fiber diameter is 17.8 μm. Injection liquid was a mixture of water/glycerol/surfactant (WGS). The characteristics of the test liquid are listed in Table 1.

Rectilinear injections were performed through the length of the preform. Constant injection pressure was applied at the injection port by an injection system where the injection pressure can be adjusted in a range from 0 to $3 \times 10^5$ Pa.

We introduce the principle of the sensor system for a real time void measurement in the subsequent section.

### 3.2. Electric conductivity sensor

The principle of the sensor system is the measurement of the electric conductivity of the liquid passing by between two parallel electrodes.[25] An electrically conductive liquid is injected into the mold containing a glass fiber preform whose electrical conductivity is low. If the injection liquid passing between the electrodes contains air voids which are insulating material, the electrical voltage will drop and this voltage drop can be correlated with the air void content. The sensors are composed of two electrodes whose dimensions are 60 mm × 5 mm × 0.05 mm and glued on the upper and lower mold platens. The electric power consists of an alternative voltage with amplitude of 10 V and frequency of 100 Hz (see Figure 4). The voltage is measured at the reference site and the voltage data are acquainted with time by Labview software (National Instrument).

For the convenience, we adopt a concept of degree of saturation instead of void content. Degree of saturation is defined by a ratio of volume occupied by the liquid to the total pore volume in the porous medium. It has been shown in the literature that the voltage value measured at the reference resistor is approximately proportional to the degree of saturation.[25] For the sensor calibration, the maximum voltage value without air voids should be decided for each sensor. Once this value is known, the degree of saturation at a fixed position can be obtained with time during the liquid injection process.

Table 1. Properties of injection liquids.

| Test liquid | Viscosity (mPa s) | Surface tension (mN/m) | Contact angle (°) |
|---|---|---|---|
| Water | 1 | 72 | ~0 |
| Glycerol | 1490 | 63 | 80 |
| WGS | 132 | 47.0 | 45 |

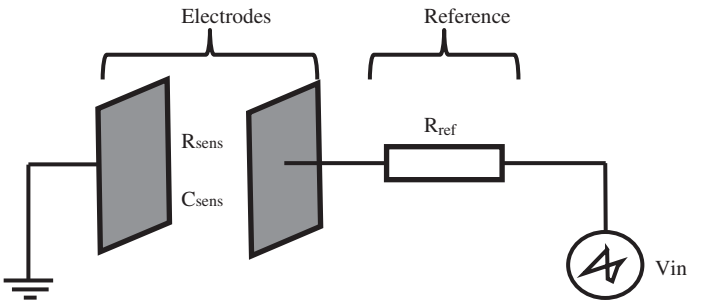


Figure 4. Schematic of circuit composition of sensor system ($R_{sens}$: Resistance of electrodes, $R_{ref}$: Resistance of reference, $V_{in}$: Input voltage).

$$S(t) = \frac{V_{\text{mea}}(t)}{V_{\text{max}}} \tag{9}$$

where $S$ is the degree of saturation, $V_{\text{mea}}(t)$ is the voltage measured at the reference resistor and $V_{\text{max}}$ is the maximum voltage value of each sensor. The maximum voltage value of each sensor is determined *in situ* by increasing the injection pressure to compact the air bubbles in the mold while the air vents are closed. The air bubbles which are entrapped between or in the tows may be compressed or expanded and their volume variation can lead to a variation of the voltage measured on the reference resistor. The voltage value was measured for several values of pressure. Assuming that the volume variation follows the ideal gas law, the variation of voltage can be plotted against the air volume and the maximum voltage $V_{\text{max}}$ which can be found for an air volume equal to zero. Because of inherent variation of sensor installation, the maximum voltage value can be different for the sensor location. Hence, the sensor calibration was performed independently and a different value of maximum voltage was assigned at each sensor.

## 4. Results and discussion

The electrically conductive liquid, i.e. the mixture of water, glycerol and surfactant, was injected into the unidirectional glass preform and the electric voltage was measured. During the liquid injection, inlet pressure was kept to be constant. The liquid injection was performed in the fiber direction of the preform. The single tow length was obtained by measuring the distance between the adjacent stitches of the preform. A number of experiments were performed with different injection pressure values. From the measured values of electric voltage, the time-dependent evolution of the degree of saturation or the air void content was obtained at each fixed sensor position as shown in Figure 5.

As seen in Figure 6(a), we can observe three characteristic stages in the graph of the time-dependent evolution of degree of saturation. Before the liquid flow front arrives at the sensor location, the voltage and the corresponding degree of saturation are zero. At the first stage (Figure 6(b)), as soon as the liquid flow front arrives at the sensor location, the voltage and the corresponding degree of saturation sharply increase. Then, air is entrapped either inside the tow or in the open gap between tows at the flow front. Meanwhile, the liquid flow front continues to advance and leaves away from the sensor location. After an air bubble is generated and the flow front sweeps away, the increase of degree of saturation suddenly becomes slower at the second stage

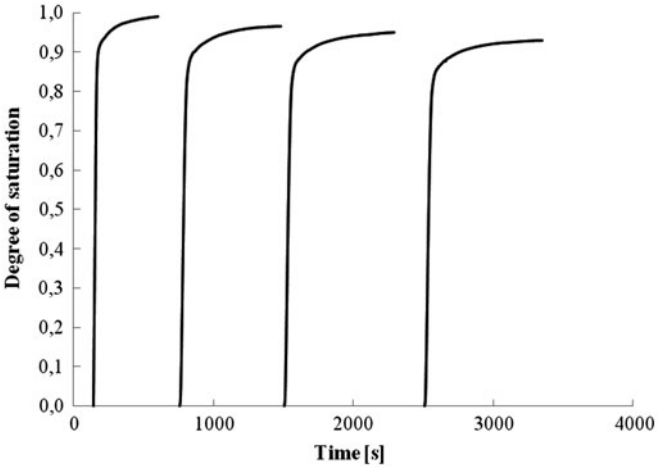


Figure 5. Examples of time-dependent evolution of degree of saturation measurement by electric conductivity sensor.

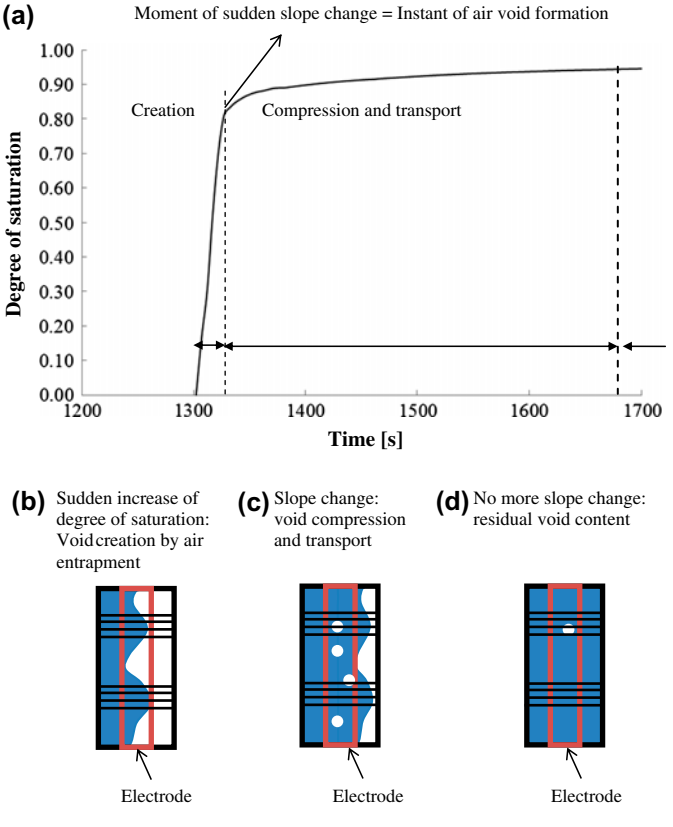


Figure 6. Determination of void formation by the evolution of degree of saturation. (a) Typical change of degree of saturation with time for a fixed position. (b) Void creation stage. (c) Void compression and transport stage. (d) Final stage (without change of residual void content).

(Figure 6(c)). During this stage, the increase of degree of saturation is driven principally by slow tow saturation or bubble compression by resin pressure increase or by bubble migration along the global liquid flow. Eventually at the final stage (Figure 6(d)), the degree of saturation does not change any more and arrives at a constant plateau when all the air bubbles that are movable have already migrated from the sensor location. From these three distinct stages of the evolution of degree of saturation, we can observe the void creation inside the preform (at the first stage) and the void transport (at the second stage) as well as the remaining void content (at the third stage).

As stated before, we can regard the moment of sudden slope change as the instant of initial void formation by air entrapment. The value of degree of saturation at this instant was obtained at each sensor and the corresponding void content was considered as the initial void content generated at the flow front. The initially generated void content was determined for each experiment when the degree of saturation did not change more than 1% per second. The instant determined in this way corresponded well to the video recordings of the liquid front advancement between the electrodes.

The experimental data were compared with the model predictions (see Figure 7). The experimental results obtained by the electric conductivity sensor are shown as solid dots in Figure 7. The results are plotted against the modified capillary number. The parameters of the preform microstructure used for the model predictions are shown in Table 2.

From Figure 7, we can see that the experimental results obtained by the sensor system show a fairly good agreement with the model prediction. It should be noted that both the experimental data and model lead to the similar results for channel void contents in terms of modified capillary number. However, the tow void content values at high modified capillary number obtained by the electric conductivity sensor were greater than those obtained by the analytical model. We can think of three reasons for this discrepancy. The first reason is assumed to be a problem of the correlation method between voltage and degree of saturation in the use of the electric conductivity sensor. The linear relation between voltage and degree of saturation (Equation (9)) was obtained by measuring the voltage drop for a given amount of glass beads which

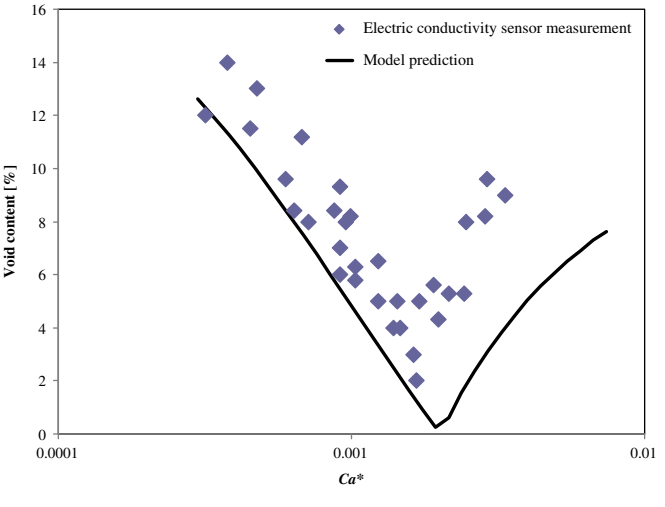


Figure 7. Comparison of experimental measurement and model prediction.

Table 2. Preform microstructure parameters for analytical modeling of void formation (Equation (8)).

| | Parameter | Value |
|---|---|---|
| $K_M$ | Macropore permeability | $6.78 \times 10^{-12}$ m$^2$ |
| $K_T$ | Tow permeability | $1.53 \times 10^{-12}$ m$^2$ |
| $V_f$ | Fiber volume fraction of preform | 0.504 |
| $L_T$ | Single tow length | 11.0 mm |
| $D_f$ | Fiber diameter | 17.8 μm |
| $v_T$ | Tow volume fraction | 0.80 |
| $V_{f,T}$ | Fiber volume fraction of tow | 0.63 |
| $h_{V,Ch}$ | Void shape factor in the channel | 1.0 |
| $h_{V,T}$ | Void shape factor in the tow | 1.0 |



simulate air voids in the liquid. Because the glass beads are spherical and remain principally in the macropore, this relation shows a good match for the channel voids which are also spherical and located in the macropore. On the contrary, the tow voids are usually cylindrical and oriented along the fiber direction inside the tow. Consequently, this relation may overestimate the tow void content. The second reason is the influence of liquid velocity on the dynamic contact angle which can change the liquid wettability and void formation.[26,27] The water glycerol and surfactant mixture are a partially wetting liquid at high velocity and the dynamic contact angle can be increased. Therefore, the wettability property and void formation may be slightly different at high liquid velocity and the corresponding high modified capillary number. The third reason is the influence of void migration. At high capillary number, air is entrapped inside the tow and only the tow void is generated at the flow front. Some tow voids continue to migrate with time inside the tow due to the high global pressure gradient, however, and some bubbles eventually escape from the tow to join the main stream resin flow in the channel. As matter of fact, the experimental data obtained by the electric conductivity sensor are the sum of tow void captured inside the tow and the channel void which was initially created inside the tow and escaped from the tow afterwards. By the analytical model, only the creation of void, either tow void or channel void, can be predicted while ignoring the void migration effect. The void migration effect is more significant at high flow rate and the model prediction may lead to an underestimation of real void content which is the sum of tow void and channel void, especially at high capillary number.

From the model prediction and experimental results, we can see that the optimal modified capillary number to minimize void formation can be analytically predicted. In the analytical model, the only parameters to decide a posteriori (e.g. fitting of experimental data or micro-image observation) are the void shape factors, viz. $h_{V,T}$ and $h_{V,C}$ in Equations (5) and (6). These parameters are not necessary, however, to predict the optimal modified capillary number which can be obtained by Equations (7) and (8). This implies that the process condition can be optimized to minimize the void formation without experimental measurement of void content, once the preform microstructure properties and the liquid properties are known.

## 5. Conclusion

We proposed the sensor system to measure the void formation not in the final cured sample but during the mold filling process. The sensor system measures the electric

voltage between two electrodes installed on the upper and bottom surfaces of the mold. Then, the electric voltage value is converted into the air void content at the sensor location. Hence, electrically conductive liquid should be injected into non-conductive preform preplaced in the mold. The analytical solution of void formation was derived based on the previous work. From the experimental measurements, we could confirm that the model predictions and experimental results showed fairly good agreements with each other. This implies that the analytical model can be useful for void minimization in real practices.

**Acknowledgements**

This work has been performed in collaboration with SAFRAN/Aircelle under the research program of 'RTM Structural'. The authors also would like to acknowledge the financial support from the French Ministry of Economy, Finance and Industry.



**References**

[1] Greszczuk LB. Effect of voids on strength properties of filamentary composites. In: Proceedings of 22nd Annual Meeting of the Reinforced Plastics Division of the Society of the Plastics Industry; 1967; Washington, DC. p. 20(A-1)–20(A-10).
[2] Hancox NL. The effects of flaws and voids on the shear properties of CFRP. J. Mater. Sci. 1977;12:884–892.
[3] Judd NCW, Wright WWW. Voids and their effects on the mechanical properties of composites – an appraisal. SAMPE J. 1978;14:10–14.
[4] Yoshida HT, Ogasa T, Hayashi R. Statistical approach to the relationship between ILSS and void content of CFRP. Compos. Sci. Technol. 1986;25:3–18.
[5] Harper BD, Staab GH, Chen RS. A note on the effects of voids upon the hygral and mechanical properties of AS4/3502 graphite/epoxy. J. Compos. Mater. 1987;21:281–289.
[6] Tang JM, Lee WI, Springer GS. Effects of cure pressure on resin flow, voids, and mechanical properties. J. Compos. Mater. 1987;21:421–440.
[7] Hayward JS, Harris B. Effect of process variables on the quality of RTM mouldings. SAMPE J. 1990;26:39–46.
[8] Hayward JS, Harris B. The effect of vacuum assistance in resin transfer moulding. Compos. Manuf. 1990;1:161–166.
[9] Lundstrom TS, Gebart BR, Lundemo CY. Void formation in RTM. In: The 49th Annual Conference, Composite Institute of the Society of the Plastics Industry; 1992; Cincinnati, OH. Session 16-F.
[10] Patel N, Lee LJ. Effects of fiber mat architecture on void formation and removal in liquid composite molding. Polym. Compos. 1995;16:386–399.
[11] Patel N, Lee LJ. Modeling of void formation and removal in liquid composite molding. Part II: model development and implementation. Polym. Compos. 1996;17:104–114.
[12] Chen YT, Davis HT, Macosko CW. Wetting of fiber mats for composites manufacturing: I. Visualization experiments. AIChE J. 1995;41:2261–2273.
[13] Rohatgi V, Patel N, Lee LJ. Experimental investigation of flow-induced microvoids during impregnation of unidirectional stitched fiberglass mat. Polym. Compos. 1996;17:161–170.
[14] Patel N, Rohatgi V, Lee LJ. Micro scale flow behavior and void formation mechanism during impregnation through a unidirectional stitched fiberglass mat. Polym. Eng. Sci. 1995;35:837–851.
[15] Ruiz E, Achim V, Soukane S, Trochu F, Breard J. Optimization of injection flow rate to minimize micro/macro-voids formation in resin transfer molded composites. Compos. Sci. Technol. 2006;66:475–486.
[16] Sejnoha M, Vorel J, Jilousek O. Mesoscopic study of textile reinforced composites. In: Proceedings of ECCM 15; Venise; 2012.
[17] Leclerc JS, Ruiz E. Porosity reduction using optimized flow velocity in resin transfer molding. Composites Part A. 2008;39:1859–1868.

[18] Park CH, Lebel A, Saouab A, Bréard J, Lee WI. Modeling and simulation of voids and saturation in liquid composite molding processes. Composites Part A. 2011;42:658–668.
[19] Park CH, Woo L. Modeling void formation and unsaturated flow in liquid composite molding processes: a survey and review. J. Reinf. Plast. Compos. 2011;30:957–977.
[20] Bréard J, Henzel Y, Trochu F, Gauvin R. Analysis of dynamic flows through porous media. Part I: comparison between saturated and unsaturated flows in fibrous reinforcement. Polym. Compos. 2003;24:391–408.
[21] Bréard J, Saouab A, Bouquet G. Numerical simulation of void formation in LCM. Composites Part A. 2003;34:517–523.
[22] Park CH, Bréard J, Saouab A, Lee WI. Unified saturation and micro-macro voids method in liquid composite molding. Int. J. Mater. Form. 2008;1:937–940.
[23] Gebart BR. Permeability of unidirectional reinforcements for RTM. J. Compos. Mater. 1992;26:1100–1133.
[24] Ahn KJ, Seferis JC, Berg JC. Simultaneous measurements of permeability and capillary pressure of thermosetting matrices in woven fabric reinforcements. Polym. Compos. 1991;12:146–152.
[25] Labat L, Grisel M, Bréard J, Bouquet G. Original use of electrical conductivity for void detection due to injection conditions of composite materials. CR Acad. Sci. II B - Mec. 2001;329:529–534.
[26] Ben Abdelwahed MA, Wielhorski Y, Bizet L, Bréard J. Characterisation of bubbles formed in a cylindrical T-shaped junction device. Chem. Eng. Sci. 2012;76:206–215.
[27] Wielhorski Y, Ben Abdelwahed MA, Biezt L, Bréard J. Wetting effect on bubble shapes formed in a cylindrical T-junction. Chem. Eng. Sci. 2012;84:100–106.